NOAA Technical Memorandum ERL MESA-38

REPORT ON FY-78 NUMERICAL MODELING IN THE STRAIT OF JUAN DE FUCA AND PUGET SOUND

C. H. Pease
R. J. Stewart
J. E. Overland

Pacific Marine Environmental Laboratory
MESA Puget Sound Project
Seattle, Washington

Marine Ecosystems Analysis Program
Boulder, Colorado
February 1979

UNITED STATES DEPARTMENT OF COMMERCE
Juanita M. Kreps, Secretary

NATIONAL OCEANIC AND ATMOSPHERIC ADMINISTRATION
Richard A. Frank, Administrator

Environmental Research Laboratories
Wilmot N. Hess, Director

Report Submitted to
MESA PUGET SOUND PROJECT
MARINE ECOSYSTEMS ANALYSIS PROGRAM
ENVIRONMENTAL RESEARCH LABORATORIES

by

PACIFIC MARINE ENVIRONMENTAL LABORATORY
ENVIRONMENTAL RESEARCH LABORATORIES
SEATTLE, WASHINGTON 98105

This work is the result of research sponsored by the Environmental Protection Agency and the National Oceanic and Atmospheric Administration and administered by the Environmental Research Laboratories of the National Oceanic and Atmospheric Administration.

CONTENTS

1. INTRODUCTION

This report summarizes and interprets tidal current and oil spill trajectory predictions obtained from a computer model of the Strait of Juan de Fuca and regional wind fields derived from a computer model of the entire Puget Basin. These models are products of a multi-year project supported by the Puget Sound MESA program. As reported here, the models are works in progress, and a final report on their development can be expected at the end of FY-79.

The meteorology of the Puget Sound Basin is discussed with respect to three dominant weather patterns which were subsequently used to run the regional meteorological model. These model results are incorporated into oil spill trajectory calculations as large scale wind fields over the Straits which are sequentially keyed by baric types for any given modeling period. A sea breeze condition was also considered and is described in the trajectory modeling section.

The oceanography of the Strait of Juan de Fuca region is presented as a discussion of the dominant features, tidal and estuarine flow components, and some possible deviations from these main elements. The tide subroutines constructed for the trajectory model are based on empirical data from NOS tidal current stations and are inline functions to the trajectory model.

For the trajectory simulations, the model included an empirical tidal current field, an approximate estuarine flow in the central and western Straits region, a time and space varying wind field, and the empirical "3% of wind velocity" oil spill trajectory equation. In order to provide regional coverage, tidal current velocities are interpolated in the computer model on a nominal one kilometer grid based on up to three neighboring tidal stations and anticipated channeling effects due to the bottom topography. The estuarine flow was approximated with a current field that was of uniform speed with direction determined by the local ebb tide direction. The wind field was modeled using both an observed surface wind time series from the Canadian meteorological station at Race Rocks and the large scale wind fields over the entire Straits/Puget Sound region. The principal product of the model was a series of simulated oil spill trajectories.

2. THE METEOROLOGY OF THE PUGET SOUND BASIN

The climate of the Puget Sound Basin is of a mid-latitude, west coast marine type. The predominant air masses reaching Puget Sound have their source regions over the Pacific Ocean, producing a moderating influence on the weather in both summer and winter. A prevailing westerly to northwesterly flow under high pressure in the eastern Pacific results in a dry season beginning in June and reaching a peak in midsummer. In the late fall and winter the high retreats to the south allowing a series of storms to cross the state producing a wet season, reaching a peak in winter and decreasing in the spring.

Topography plays a large role in influencing the weather of Puget Sound. The Puget Sound Basin is flanked to the west by the Olympic Mountains and to the east by the Cascade Mountains. The elevation varies from sea level at the Sound to 2500 m and higher in the mountains. The Cascades (and the Rocky Mountains) shield Puget Sound from winter season cold air masses moving southward across Canada. To the west, the Willapa Hills, the Olympic Mountains, and the coastal range on Vancouver Island are effective in protecting the area from more intense winter storms by forcing orographic precipitation on these western slopes. The Strait of Juan de Fuca, the Strait of Georgia, and the Chehalis River Valley provide low level passages for maritime air moving inland.

2.1 Climatological Overview

Maritime air reaching the Washington coast in late fall and winter is moist and near the temperature of the ocean surface. Orographic lifting and cooling of air masses moving inland result in cloudiness and widespread precipitation. The driest sections of the Sound are in the lee of the Olympic Mountains for southwest winds. There are two periods of high river and stream flow each year. One occurs during the fall and winter coinciding with the season of maximum precipitation. The other occurs in late spring and early summer, caused by melting snow in the mountains augmented by rainfall.

The mountain barriers and the low level passages between them influence the Puget Sound wind patterns. Figure 1 shows the surface wind roses for Washington stations. This figure must be interpreted with some care because the strongest winds at each station do not necessarily occur with the same synoptic event. In lower Puget Sound the strongest winds are from the south to southwest as the more intense Pacific storms move inland. During winter, the build up of high pressure over the interior can produce a strong easterly jet through the Strait of Juan de Fuca (Reed, 1931). It is not unusual to have south or southwesterly winds over southern Puget Sound while strong northwesterly winds are reported over northern Puget Sound and through the Strait of Juan de Fuca. In summer winds are light, developing a northerly breeze over Puget Sound and the lowlands, and a westerly sea breeze in the Strait of Juan de Fuca in the afternoon. Over the central basin extremes in wind speed can be expected to exceed 25 ms^{-1} once in 2 years, 40 ms^{-1} once in 50 years and 45 ms^{-1} once in 100 years.

2.2 Synoptic Characteristics

Throughout the winter the synoptic situation over Puget Sound is characterized by cyclonic disturbances moving over the region or to the north of the region, interrupted infrequently by anticyclones. Spring and autumn are transition periods where the frequency and intensity of the cyclones diminishes and increases respectively. The summer is marked by light cyclone activity with long periods of anticyclonic influence.

Cyclone tracks for the northeast Pacific indicate that most of the air effecting Puget Sound has its origin in the central Pacific or the Gulf of

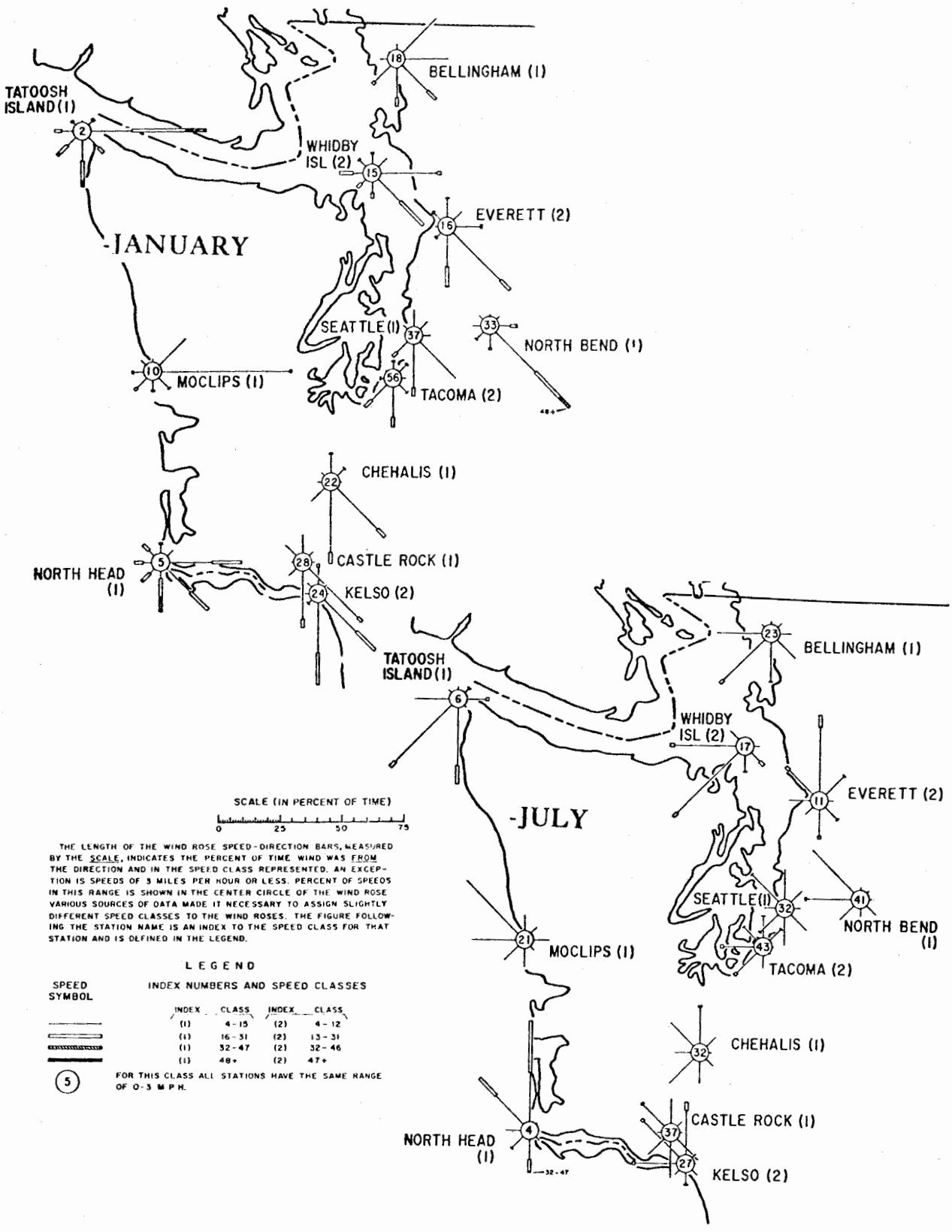

Figure 1: Surface wind roses for Washington stations for January and July (adapted from Phillips, 1968)

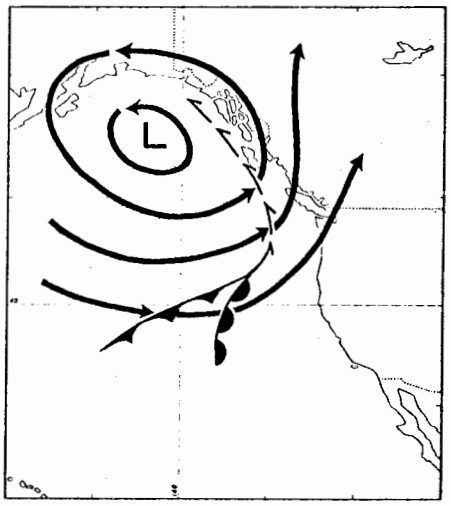

Figure 2: Weather pattern L1 (adapted from Maunder, 1968)

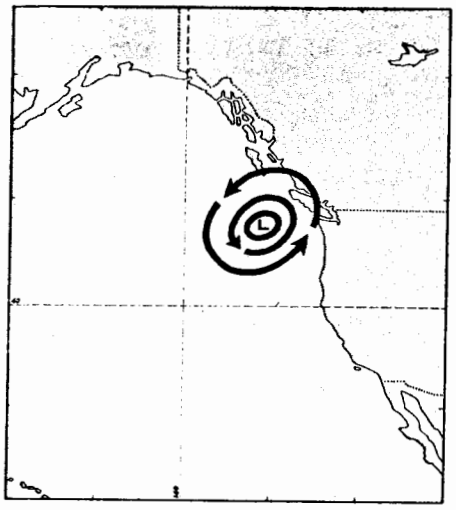

Figure 3: Weather pattern L2 (adapted from Maunder, 1968)

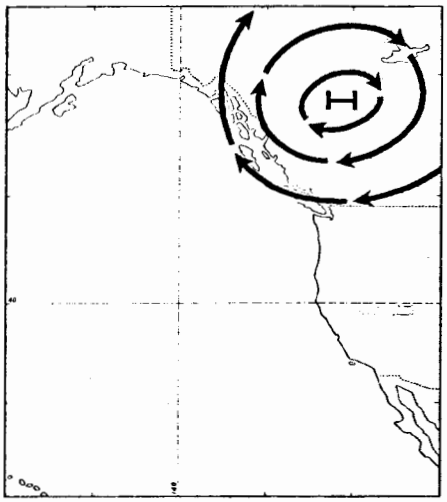

Figure 4: Weather pattern H1 (adapted from Maunder, 1968)

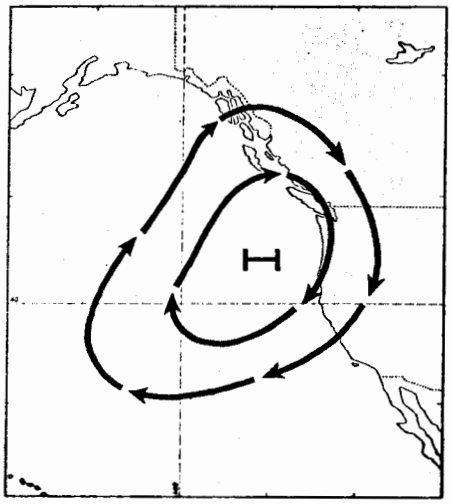

Figure 5: Weather pattern H2 (adapted from Maunder, 1968)

Alaska. While it is difficult to generalize all weather maps, two typical storm systems suggest themselves. In the first type, L1, pressure patterns are associated with a large and extensive low pressure area in the Gulf of Alaska (Figure 2), with accompanying frontal systems in the vicinity of Vancouver Island. The center of the low pressure is usually nearly stationary with the frontal systems moving rapidly across the Pacific. The warm sector of the cyclone is usually small by the time it reaches the vicinity of the coast making warm fronts in the area often weak and difficult to locate. Often the cold front in L1 will rapidly approach the coast, stall, dissipate offshore and then move over Puget Sound, so that the severity is not what would be expected from the severity over the Pacific. The timing of the inland movement of such fronts leads to difficulties in making forecasts. The second type of storm, L2, are small disturbances that form in the Central Pacific between the Aluetian low and the central Pacific high and skirt across the Pacific on an east-northeast trajectory (Figure 3), commonly landfalling over Vancouver Island. Such systems are steered by a strong westerly component in the flow at upper levels. Occasionally the large scale pattern of upper air will shift as in winter 1976-77 when storms were steered to the south of Oregon. For frontal systems associated with low pressure centers passing to the north of Puget Sound the general pattern for surface winds is prevailing south to southwesterly flow backing to west-northwest as the cold front passes through. The air ahead of the front is relatively warm and moist. Behind the cold front the weather is usually clear, often times with strong gust winds. However, this general sequence is often changed by intensification or decay in the storm system as it moves over Puget Sound or by a series of systems moving over the Sound in rapid succession along the Central Pacific track.

At some time during most winters an upper level ridge of high pressure will develop over northwest Canada. This is accompanied by a surface high over the Puget Sound region (type H1, Figure 4). The corresponding weather in Puget Sound is clear skies, due to the subsidence incurred by the high pressure area, temperatures below freezing, and very stable air in the surface layer.

The summer season in Puget Sound is still highly influenced by the effects of marine air moving over the region. Around the end of June through August the synoptic situation is characterized by a high pressure system influencing the area (type H2, Figure 5). This high pressure influence leads to the dry season with many clear days and warm temperatures and the prevailing winds are from the west to northwest. Cyclonic disturbances still come through, but their severity is greatly lessened and their frequency is likewise diminished.

The spring season is not significantly different than winter except that temperatures begin to rise and the frequency of cyclonic distrubances decreases and their distribution over time is irregular. The strength of the upper level flow diminishes in intensity as spring progresses.

The autumn season is another transition period. A common characteristic of early autumn is an "Indian Summer," the continuing influence of a high

pressure system in the area. Under this influence, the warm temperatures and clear skies of summer persist, and as the season progresses, and if the ridge still holds, gives way to cooler temperatures, producing brisk days and frosty nights. The high pressure ridge eventually breaks down shifting to the prevailing winds southwesterly and strengthening of the upper level flow. With this comes the cyclones and fronts associated with winter.

Frequency of occurrence of these major map types are summarized by Table 1. Table 1 is adapted from a study by Maunder (1968) in which two years of surface daily weather maps for the years 1964 and 1965 were classified. For December through February lows predominated over highs three to one with L1 forming 62% of the observed lows. By contrast the summer months, July through September, are dominated by H2 on 89 of 184 days compared to 71 days for all types of low pressure. On 430 of the 731 days in the two year study there was either a southwesterly flow associated with an Alaskan low pressure trough (207 days) or northwesterly flow associated with the north Pacific high (223 days).

2.3 Mesoscale Response

The surface features associated with synoptic scale weather patterns show substantial deviation from the large scale view. The predominant factor is the presence of the Cascade and Olympic Mountains. Precipitation is enhanced by orographic lifting and reduced by an effective rainshadow in the lee of the Olympics. The interaction of the tendency for channeling and the inertia of the onshore airflow induces mesoscale pressure patterns accompanied by complex wind patterns. The distribution of topography also alters the character of frontal features as they sweep across the state. Mesoscale features can effect the behavior of large scale systems in ways that are not clearly understood. For example, it is not known what the quantitative importance of the continent is in steering approaching storms or what is the importance of the distribution of elevation, roughness and heat and moisture sources on storm development. The following paragraphs illustrate the regional wind pattern for three quite different synoptic cases, a storm approaching from the Pacific, a wintertime fair weather case with a high positioned to the east of the Puget Sound, and a summertime offshore high pressure.

The synoptic situation of 0000 GMT, December 8, 1976, is typical southwesterly geostrophic flow before the passage of a cold front (Figure 6). Soundings at SEATAC showed a well mixed boundary layer to 1500 m. The local wind field (Figure 7) shows flow channeled by the Olympic and Cascade Mountains. The winds over Puget Sound are stronger and more southerly than offshore. In the lee of the Olympics, a region of light winds is evident. Simulation of this event with a simple meteorological model (Overland, 1978) suggests that the airflow overtops the west end of the Olympic Mountains and inertia carries the flow toward Vancouver Island. This flow and the flow north through Puget Sound creates an eddy and downward motion in the vicinity of Port Angeles. Further simulations show that the position of this eddy is very sensitive to the direction of geostrophic onshore flow.

TABLE 1

MONTH

Weather Pattern	J	F	M	A	M	J	J	A	S	O	N	D	Total Year
L1	27	19	14	24	13	8	10	10	9	27	20	26	207
L2	17	7	22	20	11	11	8	13	12	7	25	21	174
H1	8	3	6	0	1	1	1	2	5	11	6	3	52
H2	6	27	15	13	25	29	31	27	31	9	4	6	223

Frequency of occurrence of four major weather map types for the years 1964 and 1965 (adapted from Maunder, 1968)

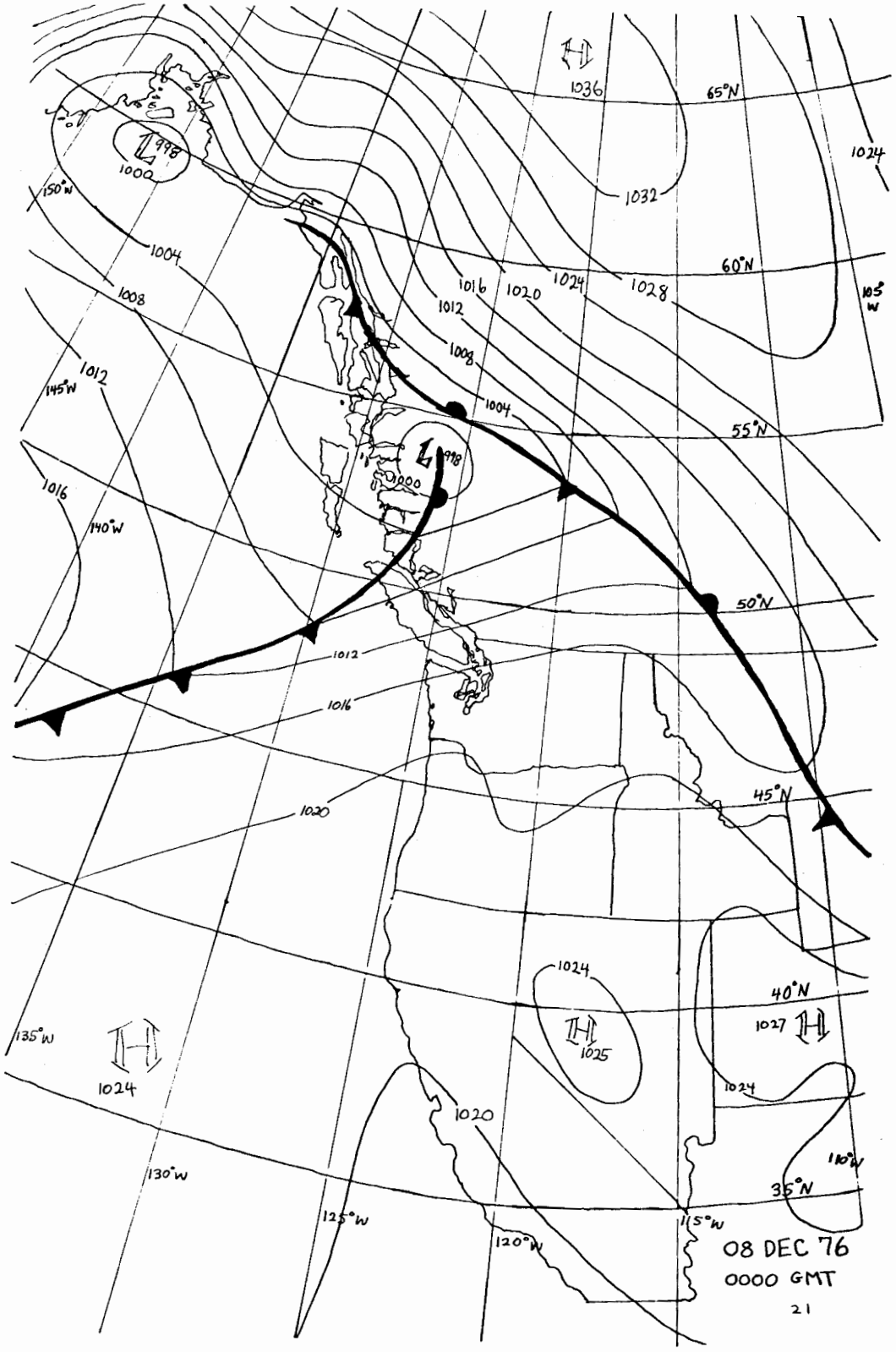

Figure 6: Example of southwesterly geostrophic flow before the passage of a cold front on 08 December 1976

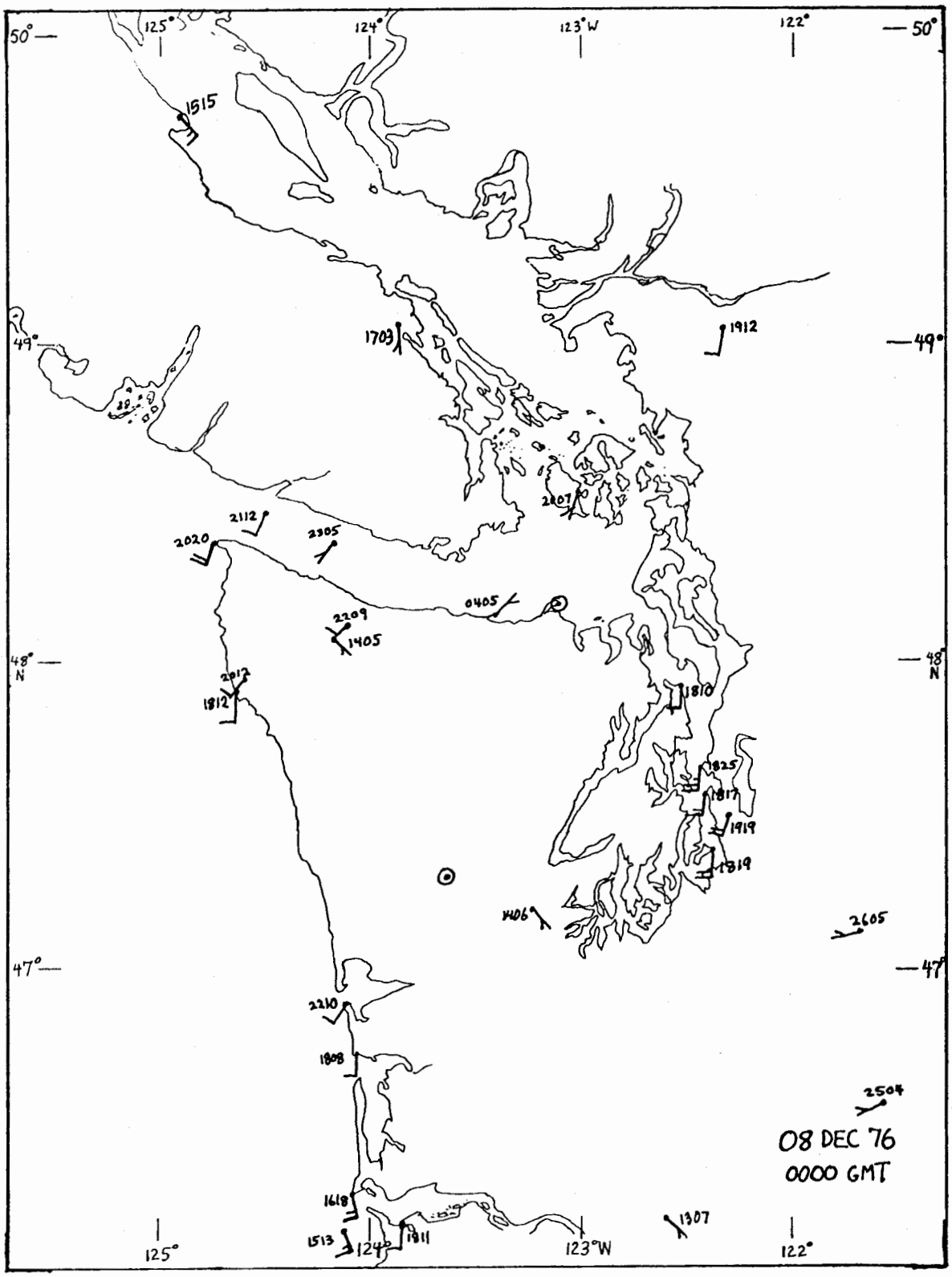

Figure 7: Local wind field for 0000 GMT on 08 December 1976. One barb represents 10 kits and a half barb represents 5 kts

To the north, a general steerage of flow along the axis of Georgia Strait is seen, more than 90° deflection of the geostrophic wind.

A second example is high pressure in the continental interior with clear skies and relatively low winds at 0000 GMT on December 1, 1976 (Figure 8). Soundings at SEATAC show strong stable stratification in the lower layers of the atmosphere. Widely spaced isobars would suggest weak flow outward from the high pressure center westward over the area. However, with the presence of topography the local wind, as shown in Figure 9, reveals a complex pattern with easterly winds at the coast and calm or light northerly winds in Puget Sound. In sharp contrast to the weak and variable winds elsewhere on the inland waters, there is a strong flow out the Strait of Juan de Fuca reaching 20 kts at Cape Flattery. These are the "gap winds" to which Reed (1931) refers. He documents cases as great as 40 kts, well in excess of a geostrophic wind magnitude. For this case the meteorological model suggests outflow at the surface, south through Puget Sound, west through the Strait of Juan de Fuca, and northwest through the Strait of Georgia with the air being replaced by vertical subsidence in the high pressure. Flow in the Strait of Juan de Fuca is accelerated down the pressure gradient with little impediment by surface friction and spills out over the Pacific.

Typical of the mid-summer synoptic situation is a high in the Pacific off of the Oregon coast bringing northwesterly winds through Washington as part of the anticyclonic circulation. This situation also occasionally occurs during late fall (Figure 10). The topography again diverts the northwesterly wind (Figure 11). Strong channeling is seen in the Strait of Juan de Fuca with variable winds in the lee of the Olympic Mountains.

Superimposed upon this mean flow during the summer is a strong diurnal signal associated with a seabreeze. Staley (1957) described the diurnal variation of the local winds by computing the resultant wind from separately averaging the north and east components over 31 days in July 1950 for each hour of the day. The result gives hodographs of the diurnal cycle as shown in Figure 12 for Victoria, Port Angeles, Everett, SEATAC, and Olympia. Victoria and Port Angeles show continuous component from the west with a maximum near 1800 local time. Everett shows much lighter winds than the Strait with near stagnation in the early morning, building to a northerly wind as the lands warm throughout the day. SEATAC is in the lee of the Olympics for northwest offshore flow. The hodograph suggests near zero mean with a "sound" breeze building in the afternoon between 1200 and 1500. The hodograph at Olympia is badly scrambled but definitely shows diurnal variation with a net flow from the southwest around the Olympic Mountains.

3. OCEANOGRAPHY OF THE STRAITS AND SAN JUAN ISLANDS

Tidal currents are probably the most obvious feature of the surface currents of the Straits of Juan de Fuca and Georgia and the interconnecting channels around the Gulf and San Juan Islands. The topology of the region is complex and the response to tidal forcing is intricate, although reasonably cyclic. These characteristics make the area both difficult to

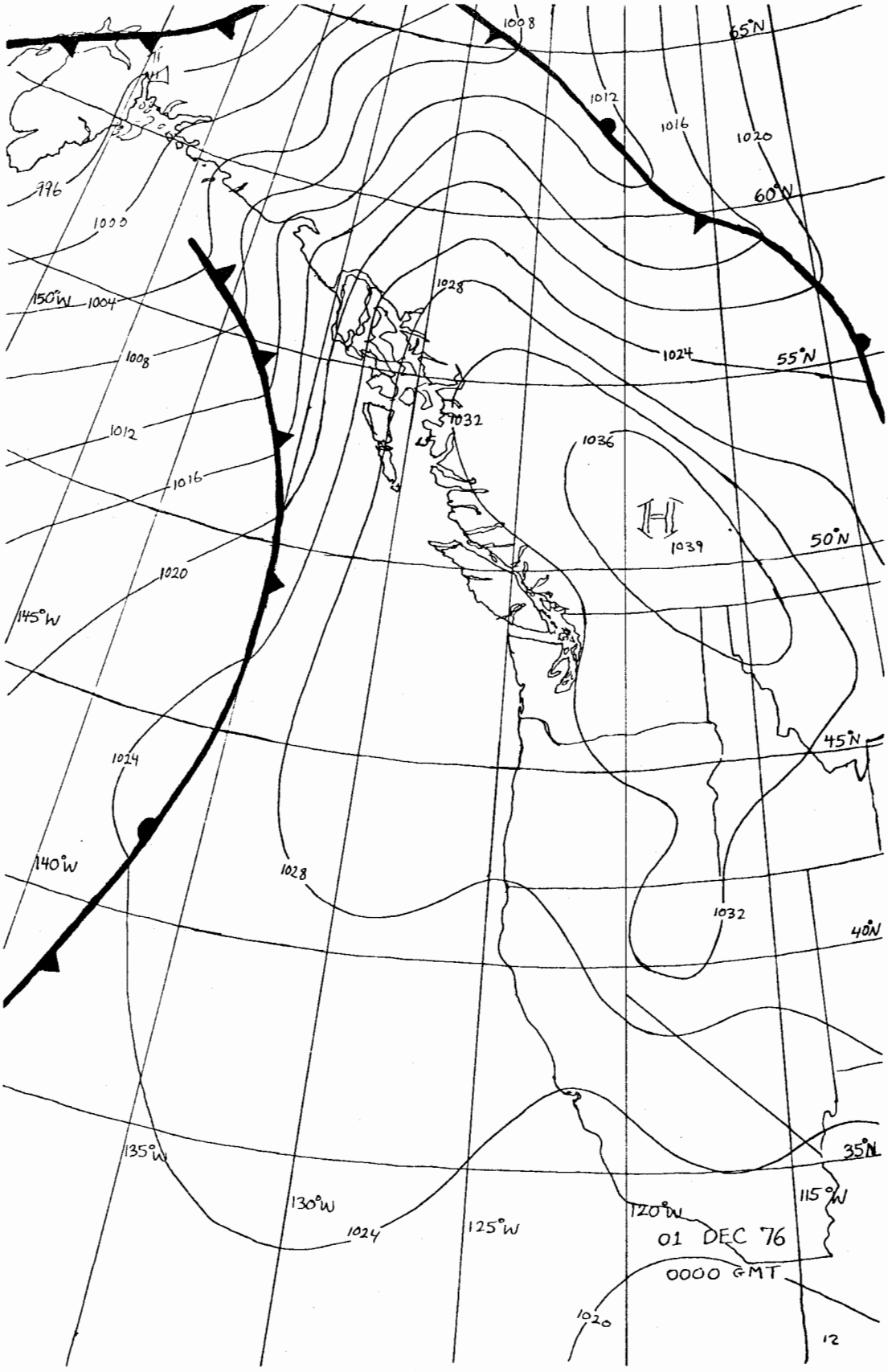

Figure 8: Example of high pressure over the interior with low winds on 01 December 1976

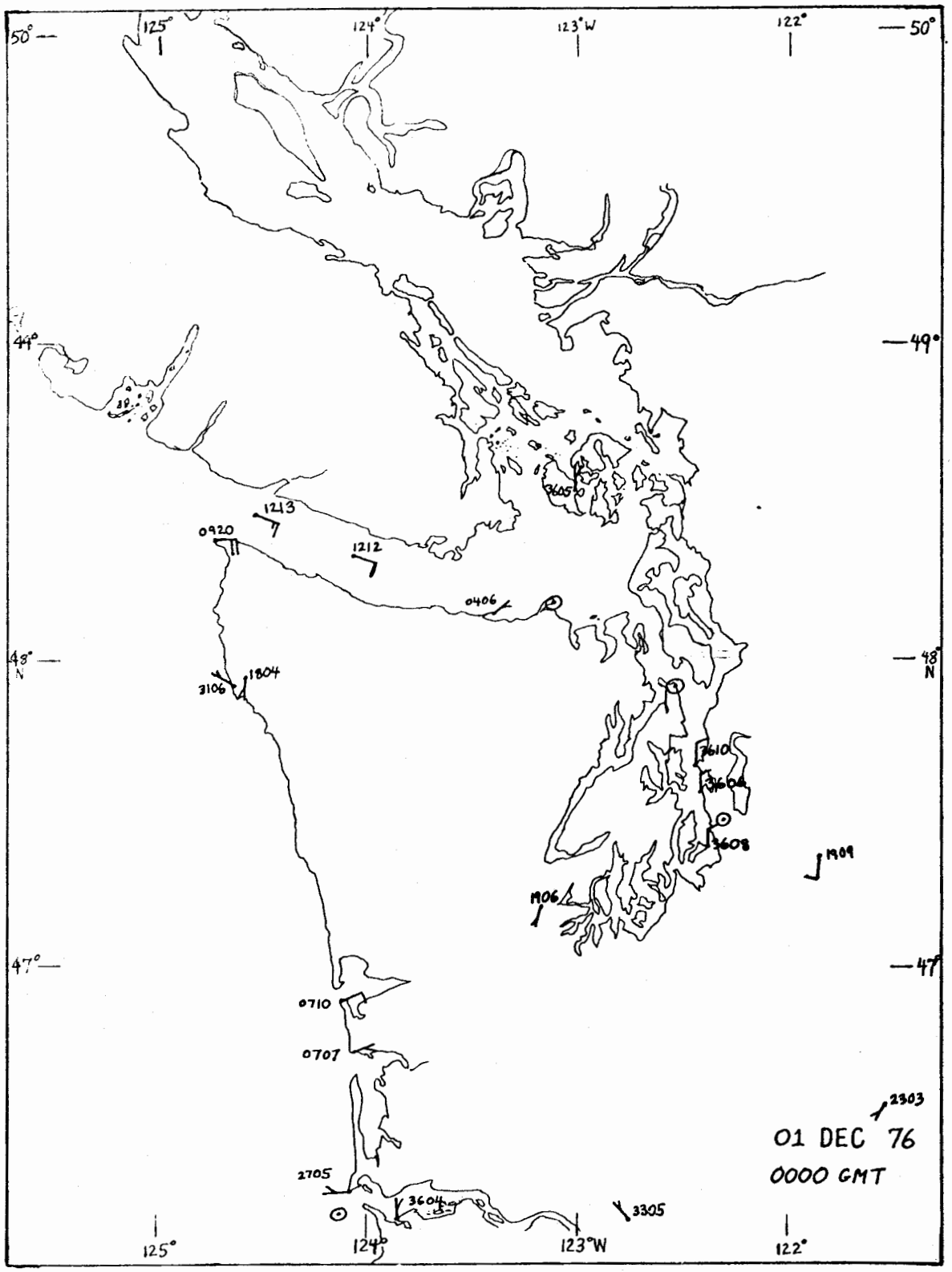

Figure 9: Local wind field for 0000 GMT on 01 December 1976

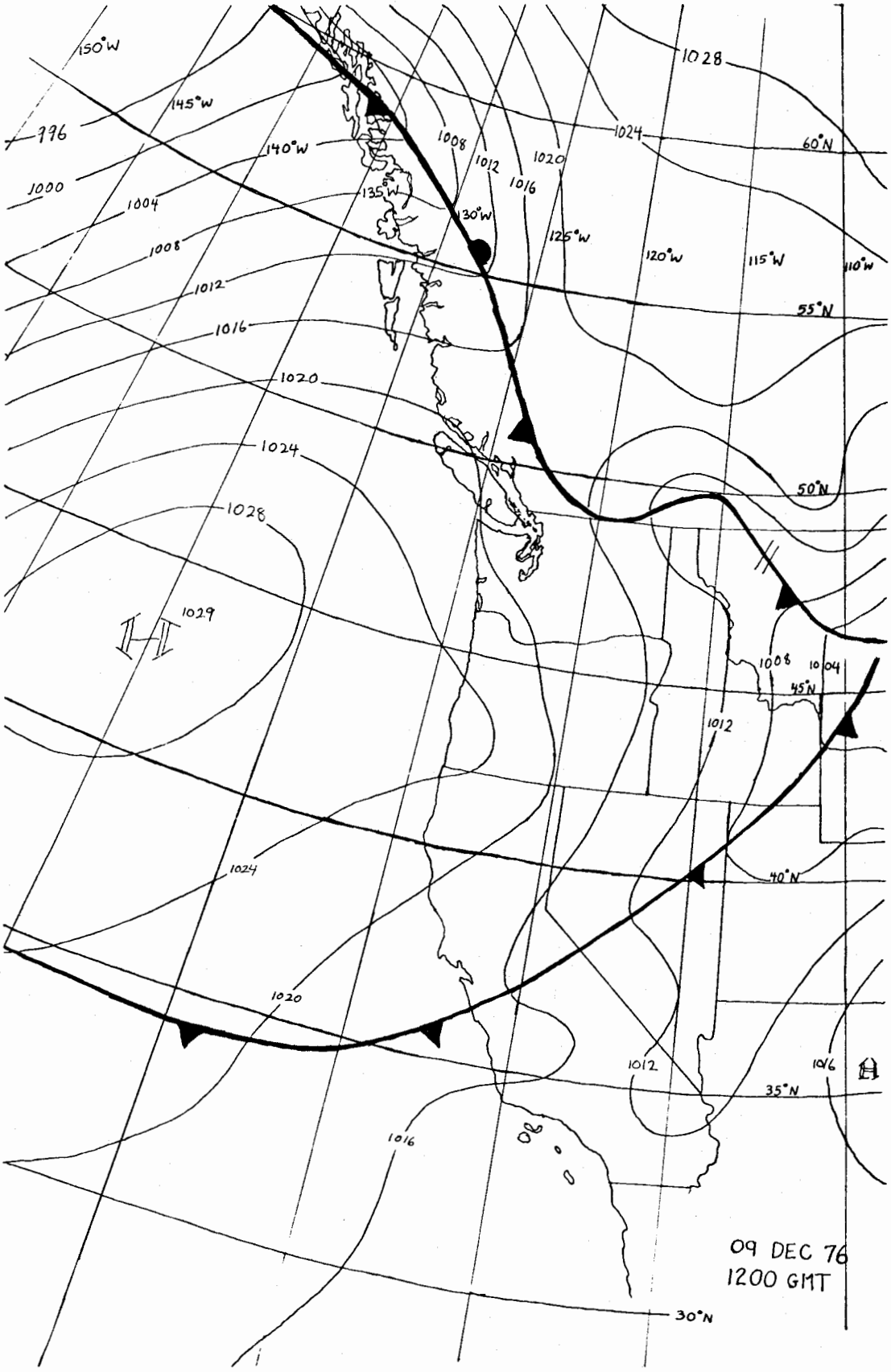

Figure 10: Example of high pressure off the Oregon coast with northwesterly winds on 09 December 1976

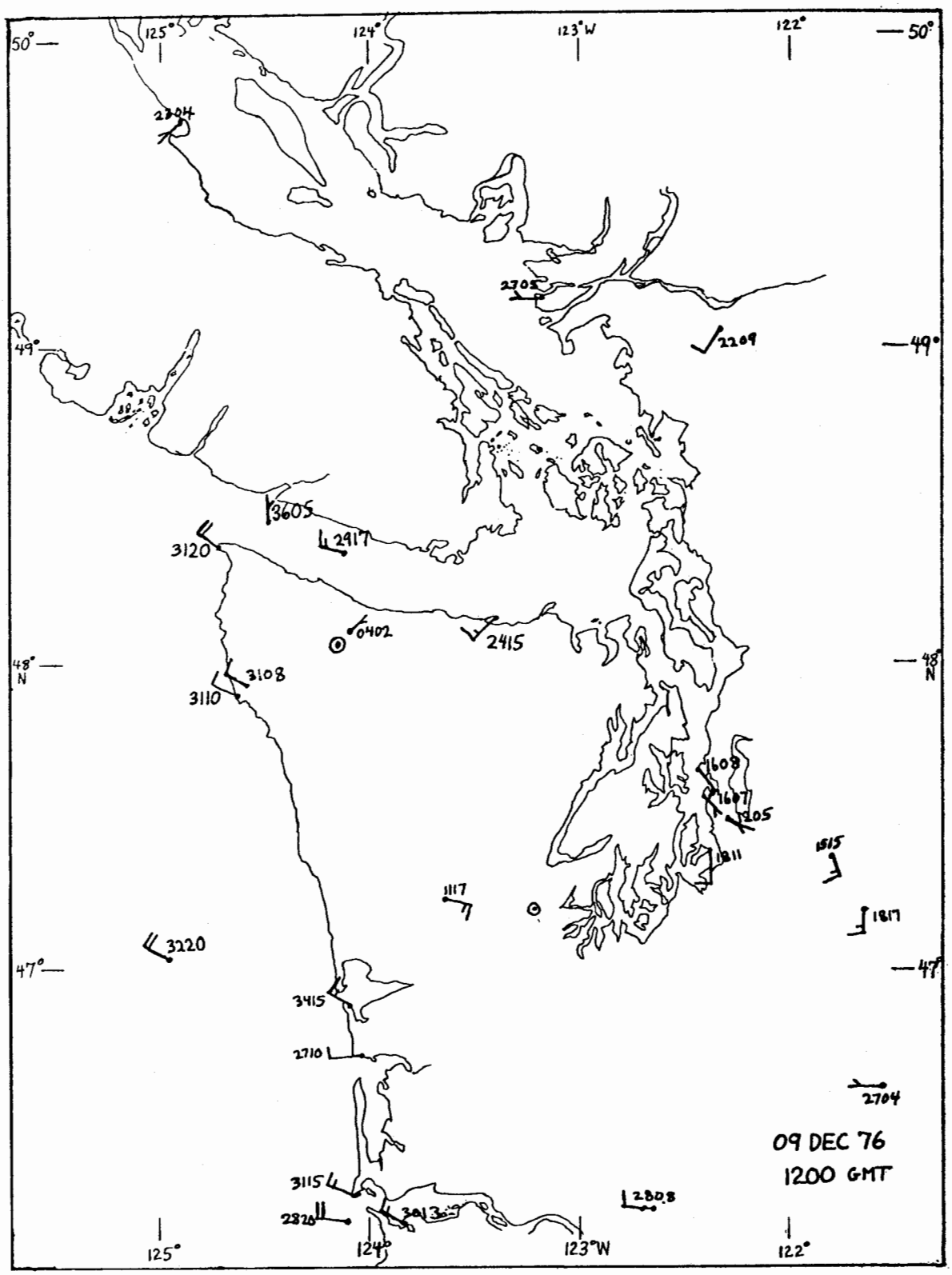

Figure 11: Local wind field for 1200 GMT on 09 December 1976

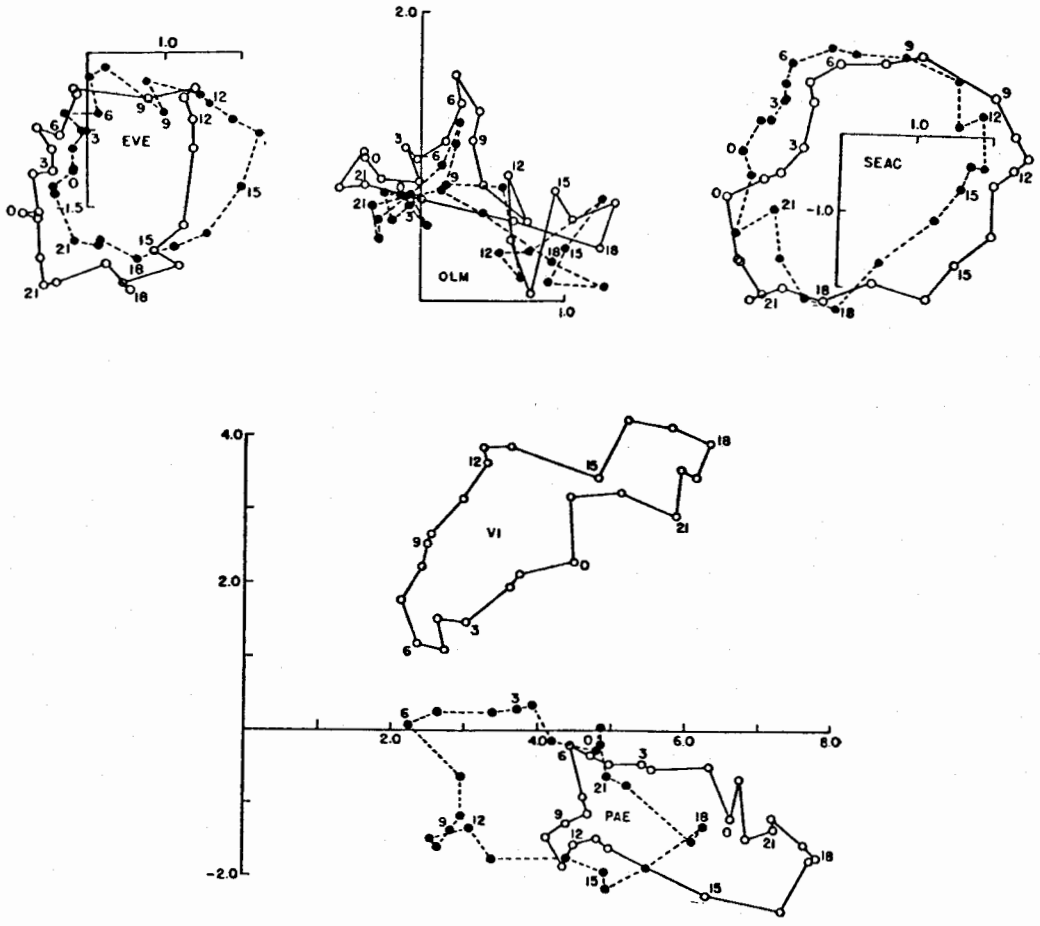

Figure 12: Hodographs for July and August 1950 at Everett, Olympia, Seattle-Tacoma airport, Victoria and Port Angeles. The observations are valid 20 minutes past PST hours indicated. Solid lines and open circles represent July values and dashed lines and dots represent August (adapted from Staley, 1957)

understand spatially and relatively straightforward to understand temporally.

Although there is a large body of literature devoted to the harmonic analysis of tides at a point in space and devoted to tide models based on principles of hydrodynamics for limited areas or geometrically simple regions, there is very little material devoted to the response of large, geometrically complicated basins like the Straits-Islands region. NOS has undertaken a recent, detailed tidal current survey of this area (Parker, 1977). Ninety current stations were occupied and analyzed for the five most important harmonic constants. Harmonic constants for six reference stations taken earlier are also available from NOS. These stations and their subordinates form the historical basis for the NOS tidal current tables.

While the tidal components are a prominent feature of the currents in the region, other currents play a critical role in determining long term trajectory behavior. Cannon (ed. 1978) reviewed the present understanding of the complex oceanography of the region. He identified two major phenomena that are of potential importance to this study. These phenomena are the estuarine flow that is ubiquitous throughout the region and the cyclic pumping of the outer straits by wind-generated set-up along the west coasts of Washington and Vancouver Island.

The estuarine flow is evidenced by the complicated southerly transport of the Fraser River sediments south through the San Juan Islands and by the strong mean currents observed in the surface layer of the Strait of Juan de Fuca. In the Straits, the estuarine current appears to be strongest on the northern side of the channel. Observations of the density structure in the Straits suggest some inflow along the southern boundary. Figure 3.3.2 of Cannon (1978) shows the mean surface layer velocity in the middle of the Straits to be seaward and in the range of 10 cm/sec to 30 cm/sec in winter and 40 cm/sec in the summer. In Haro Straits, to the west of the San Juan Islands, a two layer flow system has been observed with low frequency, estuarine, southerly surface flows evident over the width of the channel, balanced by northerly transport below 50 m (Cannon, 1978, p 38). Satellite imagery has shown that Fraser River water may be carried into the Rosario Straits by prolonged northwesterly winds. This, too, will result in low frequency estuarine flows south through Rosario Straits and into the central basin. These currents can account for substantial oil spill transport. A steady thirty centimeters per second, for example, corresponds to a net motion of twenty-six kilometers per day.

The pumping of the outer Straits by the coastal set up can cause further complications in the circulation. Most simply, it can cause current reversals that propagate with decreasing strength into the Straits. This forcing apparently accounts for a substantial portion (e.g., 27%) of the low frequency variance in the along-channel flows, northerly currents being linked to outflows and southerly currents being linked with intrusions. Less directly, but also of importance, this inflow of dense oceanic waters may induce variations in the baroclinic component of the tide.

Perhaps indicative of the importance of these phenomena are recent observations of a 20 m drogue released off Dungeness (Holbrook, personal communication). This drogue was released at nearly the neap of the tidal cycle in August, and model forecasts based on tidal currents alone showed little net motion. Contrary to these predictions, the drogue showed a net motion over 45 hours of about 65 kilometers down the Straits towards the Pacific Ocean. This is consistant with a net estuarine flow of about 40 cm/sec, which is in agreement with the results discussed in Cannon.

4. TRAJECTORY MODELING OF THE STRAITS AND SAN JUAN ISLANDS

4.1 The Trajectory Model Description

The key elements of the model are the high resolution tidal current field and the large scale wind patterns. Each of these elements is based on a number of fairly lengthy and complicated submodels comprised of programs, validation procedures, and supporting data sets. Although we believe these submodels are the most representative simulations available for the Strait of Juan de Fuca region, they are approximations to the physical system. The model results are thus subject to errors and must be interpreted according to our estimates of the short-comings of the submodels.

The tidal current field model is described in Pease (in draft). The model has a nominal one kilometer resolution. Figure 13 shows the center of each grid square in the tidal current array. Tidal current amplitudes are based on interpolations between neighboring current stations. The interpolation factors were determined through an objective but non-quantitative consideration of possible channeling effects. The direction of the tidal current is either specified as parallel to the channel axis in highly constrained regions, or as the major axis of the M2 component of the tidal elipse in areas where channeling is not expected to be effective.

These simplifications of the behavior of the tidal current no doubt result in some error. Although quantitative estimates have yet to be made, we believe that the current speed error is on the order of 10% and the current direction error is generally on the order of 10°. The exceptions to this rule of thumb are in areas of temporally non-symmetric flow like those regions adjacent to a prominent point where eddies will form on one side during the ebb phase of the tide and on the other side during the flood.

The initial runs of the trajectory model were based solely on the wind and tidal current submodels. A number of very lengthy trajectories were calculated in these runs. Many of the lengthy trajectories in the middle and outer straits involved repeated tidal oscillations coupled with a weak net easterly drift caused by the wind. Because of the known (but unaccounted for) estuarine flow in this area, we judged such results to be artifacts induced by inadequate modeling of the oceanography of the region. Unfortunately, while the data and theory are adequate for such a diagnosis, they are not sufficient to provide a basis for comprehensive model along

FIGURE 13

STRAITS OF JUAN DE FUCA AND SAN JUAN ISLANDS TIDAL GRID SYSTEM(1 KM RESOLUTION)

Tidal Currents Based on NOS Measurements and Analysis

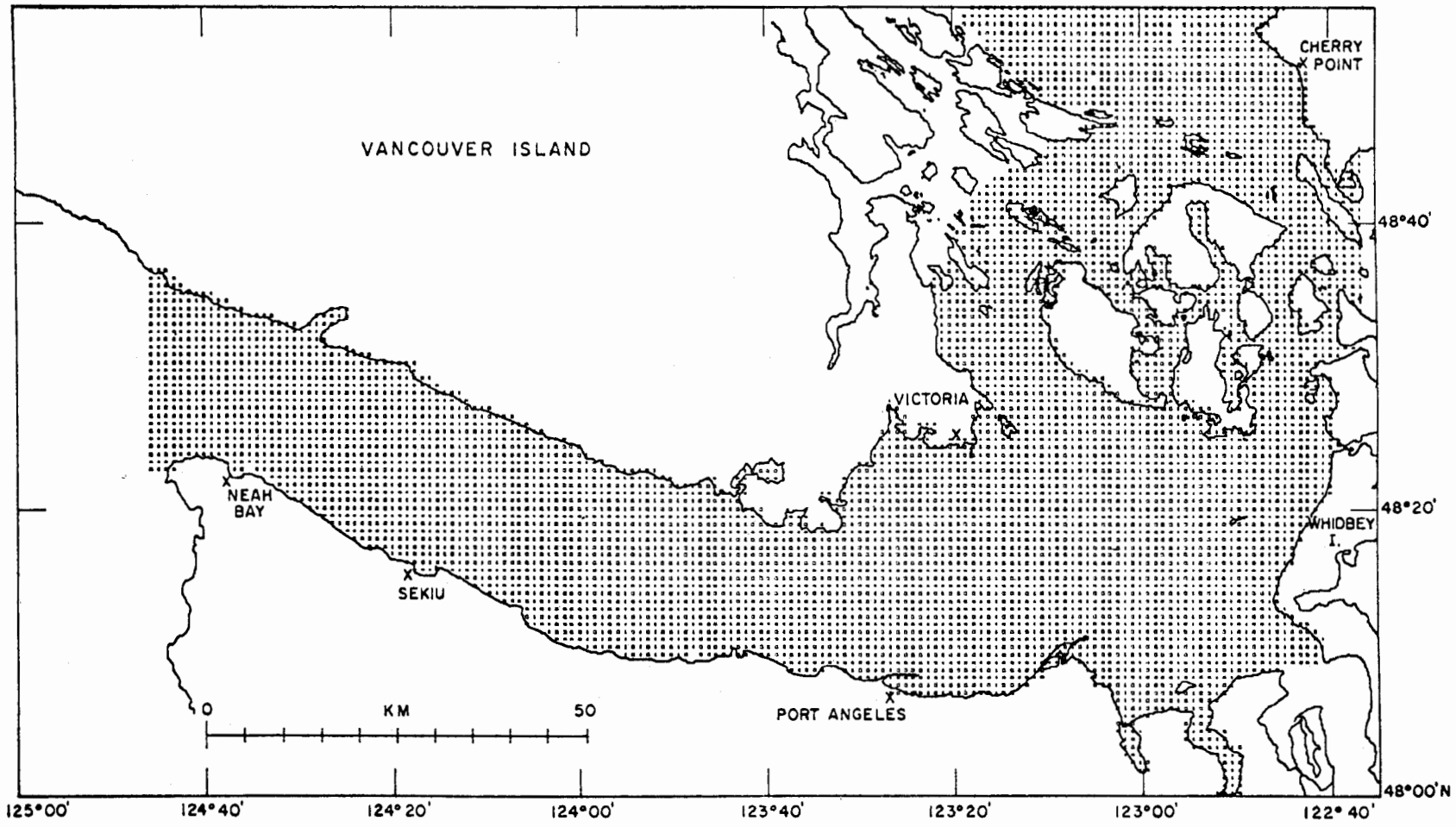

the lines of the tidal current model.

After some consideration of the problem, we decided to model the currents in middle and outer straits using two specifications. The first specification included just the oscillatory tidal component, as discussed above. The second included the tidal components plus a steady, spatially homogeneous seaward drift of 10 cm/sec in the winter and 30 cm/sec in the summer. This provides a crude representation of the estuarine flow, but it neglects the suspected transverse shear of the longitudinal current component, the transverse perturbations that accompany longitudinal variations, and the pumping of the outer straits. Therefore, the model results are not to be accepted without considerable interpretation. However, by comparing the results from both specifications, it is possible to speculate on the probable effort of the neglected variability. We did not attempt to simulate the estuarine flow in the central basin and San Juan Island regions because of the enormous spatial and temporal variability observed in these regions (Cannon, Figure 3.4.1).

There are two sources of error in modeling of the regional wind pattern, and both are of potential importance to the results we present here. First, we have not calculated wind fields for all of the characteristic patterns for the region. Thus, we do not have as good a basis for extrapolating the wind field for all of the days under consideration as we might have. The second error is that the regional wind submodel does not include locally-forced sea and land breeze effects. During fall, winter and spring, these effects are not of great importance, but in summer and perhaps early fall the seabreeze plays an important role in the wind patterns seen in the eastern Straits region. Unlike the winds shown in Figure 16, which tend to be weak in the vicinity of Admiralty Inlet, the sea breeze condition will be characterized by strong winds diverging both north and south off Whidbey Island in the vicinity of Admiralty Inlet. In order to stimulate this important feature, we have included a hand derived wind field based on wind hodograph statistics computed by Staley (1957). The sea breeze wind field is shown in Figure 17.

The trajectory model itself was rather simple as compared with the highly complicated tidal current and wind field submodels. Its function was to numerically integrate an equation of the form

$$\frac{d\bar{x}(t)}{dt} = \bar{V}_{oil} \quad (\bar{x}(t), t)$$

where $\bar{x}$ is the position of the oil spill at time t, and $\bar{V}$ is the velocity of the oil at that position and time. The resulting trajectories were then plotted on maps of the region showing travel times and places of impact.

The oil's velocity was related to the wind and current velocities at position $\bar{x}(t)$ by the formula

$$\bar{V}_{oil} = \bar{V}_{current} + .03^{*} \bar{V}_{wind}$$

FIGURE 14

REGIONAL SURFACE WINDS INDUCED BY INLAND HIGH PRESSURE SYSTEM

(characteristic Winter Pattern)

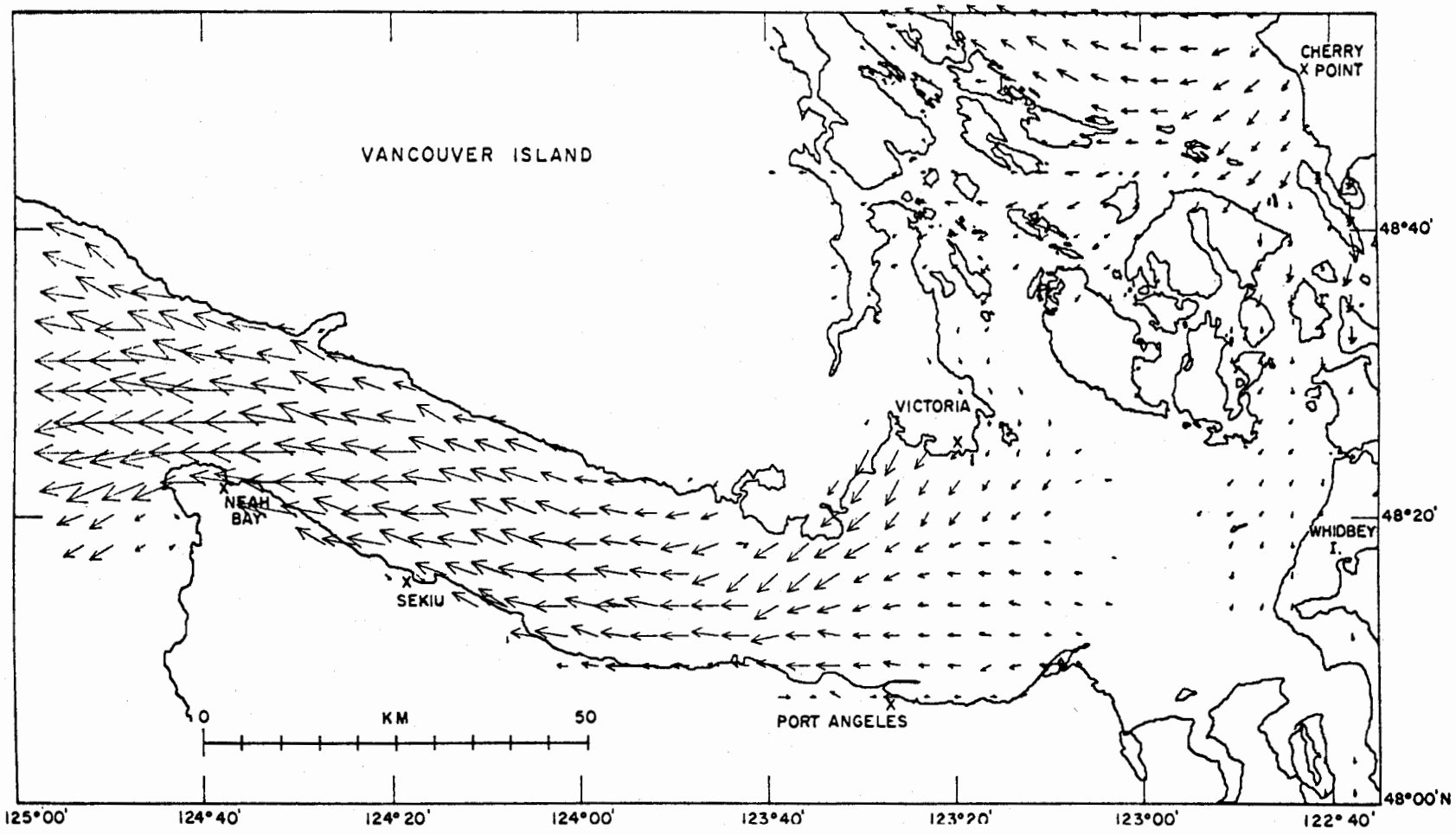

FIGURE 15

REGIONAL SURFACE WINDS DURING STORM PASSAGE

(Low Passing North of Region, Characteristic of Fall, Winter, Spring)

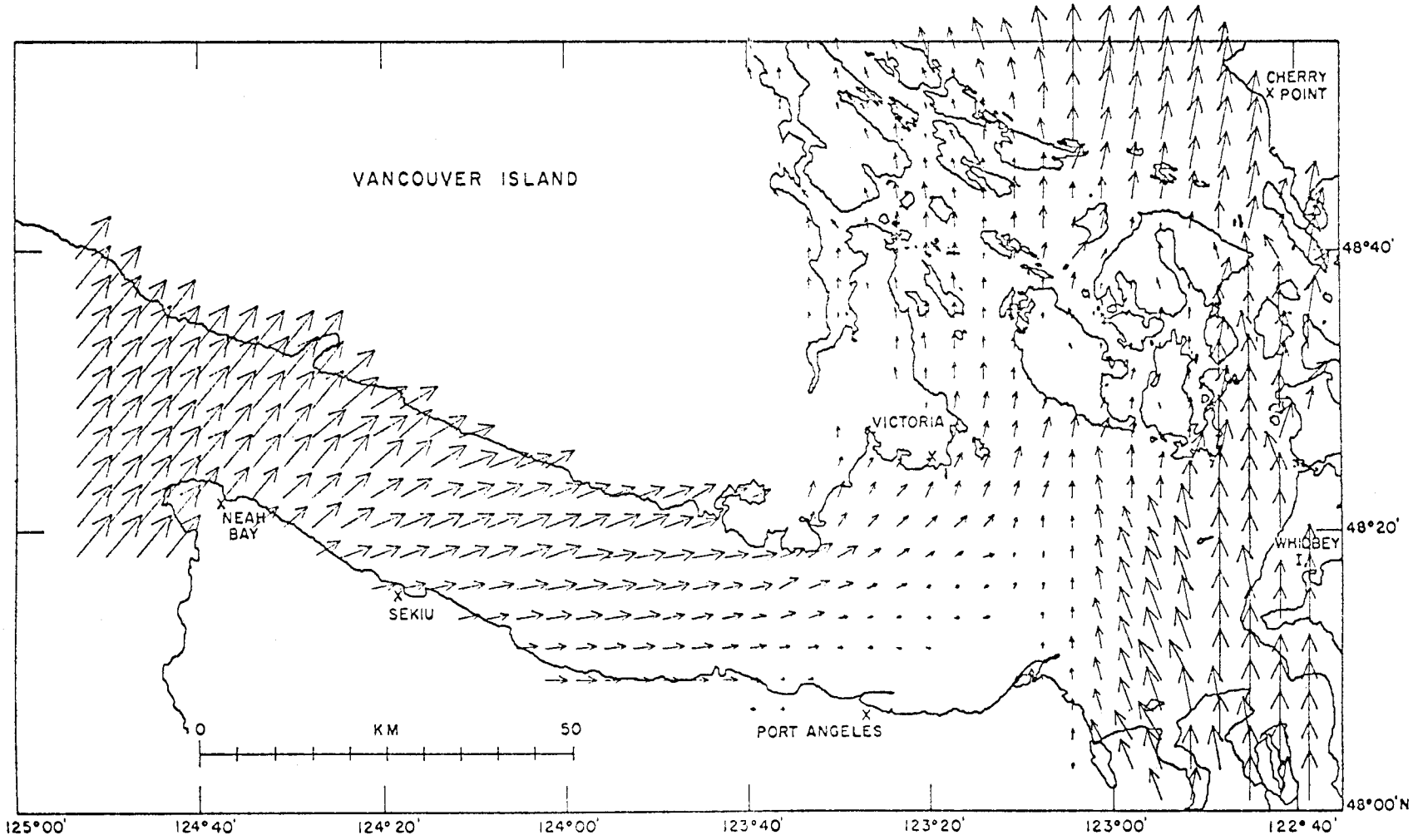

FIGURE 16

REGIONAL SURFACE WINDS INDUCED BY EAST PACIFIC HIGH PRESSURE RIDGE

(Characteristic of Summer)

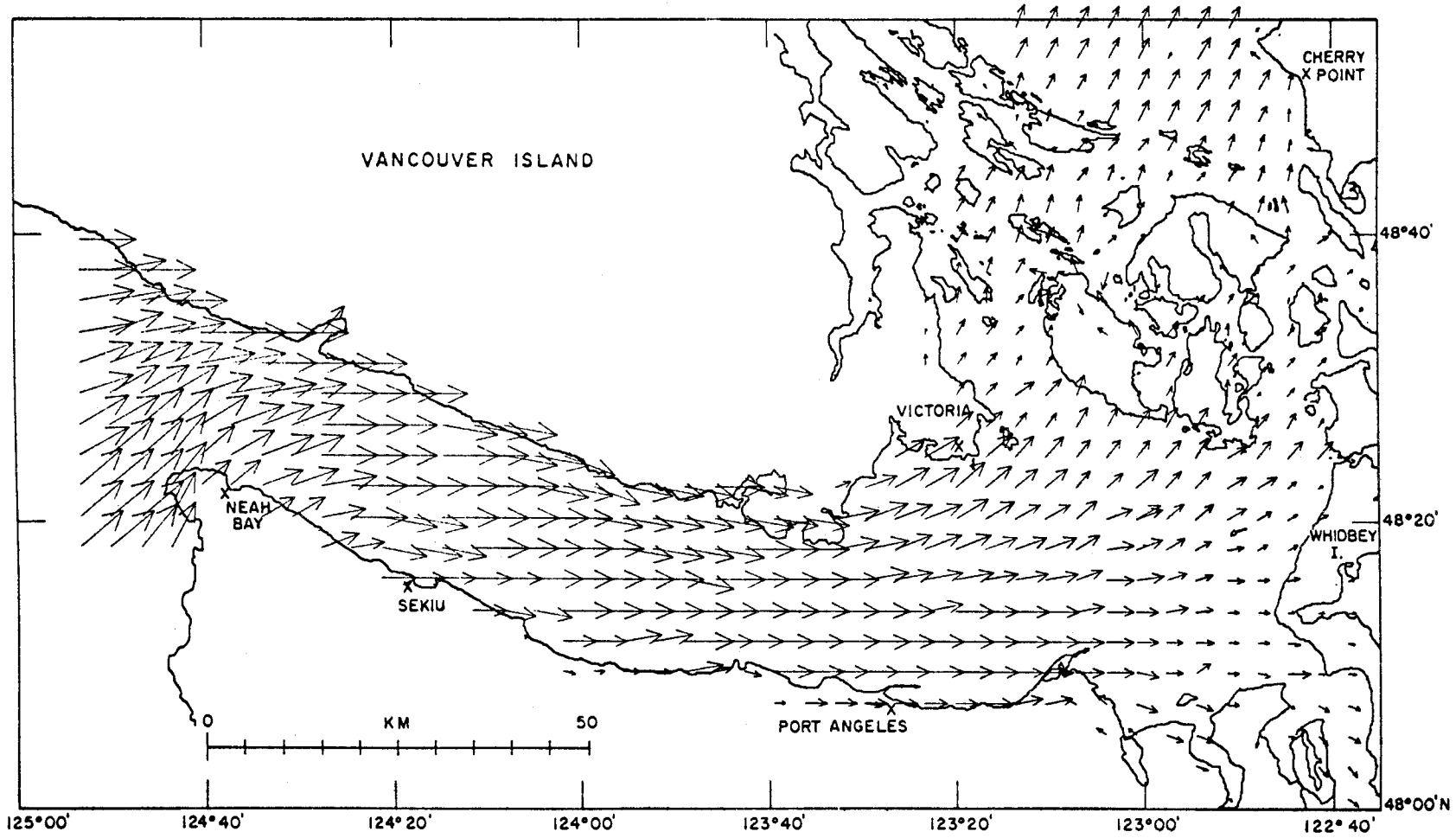

FIGURE 17

SEA BREEZE WIND FIELD

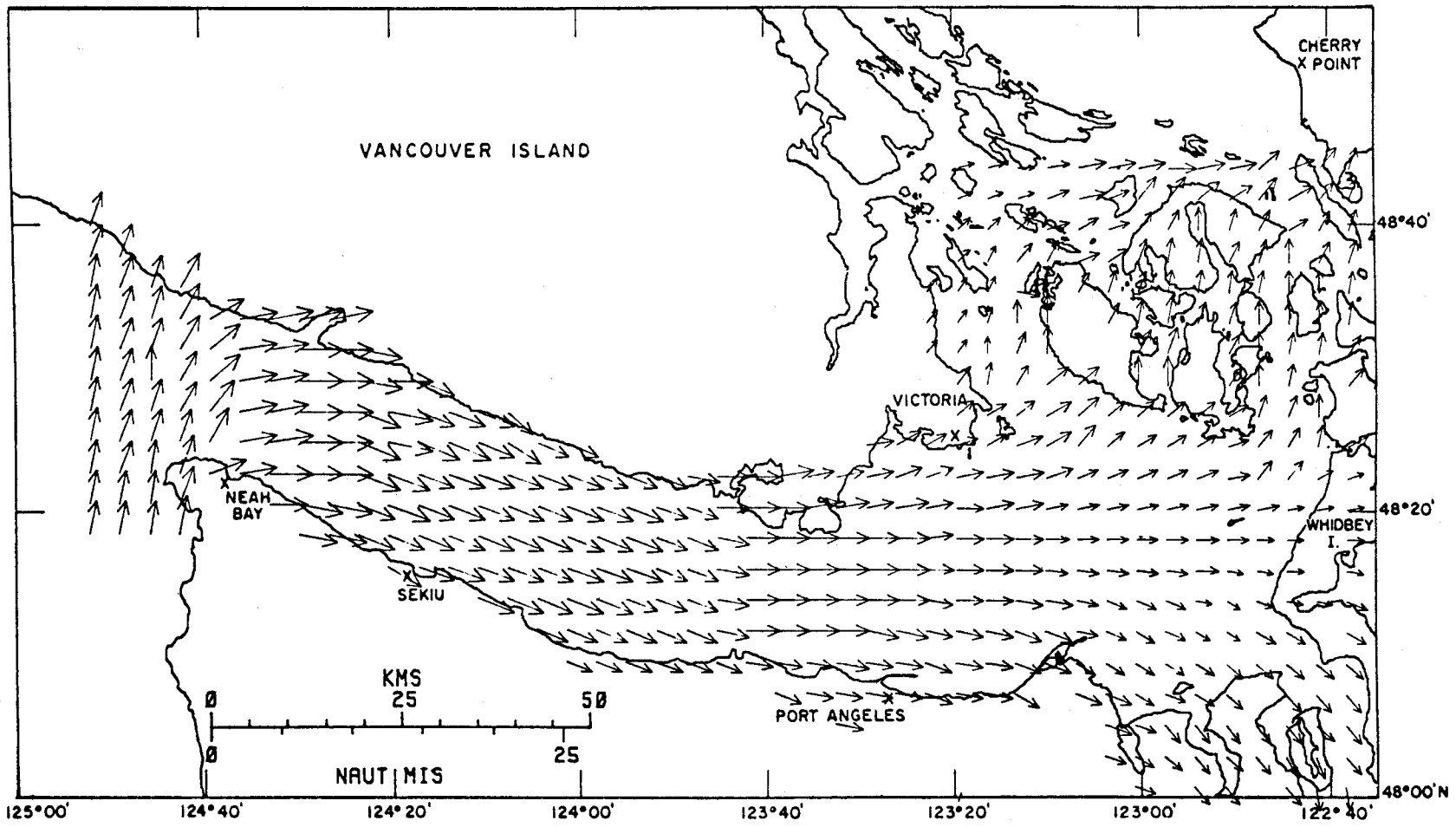

This is a generally accepted form for the equation, but its appropriatness for all conditions is questionable.

The trajectory model used one hour as its basic time step. This provides good resolution of the tidal cycle. The large scale wind patterns were assumed constant over twelve hour periods beginning at midnight. The amplitude of this large scale wind field was adjusted so that the wind field's speed at Race Rocks equalled the corresponding twelve hourly average of the observed wind speed. To inject a higher frequency, random component in the surface wind than that allowed by the twelve hourly transition between wind field types, an hourly perturbation velocity was calculated based on the difference between the hourly Race Rocks observation and the amplitude-scaled field velocity where this velocity included an estimate of the sea breeze velocity. This perturbation velocity was then scaled and added to other locations in the field. The scaling factor for any given position was the quotient of the wind field speed at the location in question and the speed at Race Rocks. Thus, areas in the wind field with low wind speeds had correspondingly small perturbations.

4.2 Trajectory Model Examples

All the simulated spills were assumed to occur instantaneously and they were tracked until they either ran aground or until we ran out of wind observations at Race Rocks. We utilized two months of hourly wind data from the Race Rocks station. The spring simulations were based on March 1976 records, and the fall simulations were based on September 1977 records. Race Rocks was chosen for the simulations both because of its central position in the region, and because its record interval was the desired one hour.

September 1977 is not an ideal month for characterizing fall winds, because of an unusually prolonged summer weather regime in that year. This summer-like weather resulted in important sea breeze affects. Consequently, the September simulation includes some features more usually found in summer. Unfortunately, we do not have any other examples of wind time series suitable for our model.

Because of the limited duration of the wind observations, the total number of trajectories was necessarily small. We estimate that three or four days must pass before the wind behaves independently (that is, it no longer feels its prior state), and so the number of quasi-independent realizations was typically seven. This means that a statistical interpretation of our results is not possible, and we caution that the trajectories can only be used to focus on the most likely regions of spill impact.

Consider the example of a spill off Neah Bay. The mechanism within the model for the northerly flow evidenced in the trajectories of Figures 18 and 19 is the turning of the wind at the Straits entrance (Figures 15 and 17). Not included are the north/south current perturbations associated with the low frequency pumping of the outer Straits by the coastal setup.

Figure 3.1.1 of Cannon shows winter and spring surface drifters from

FIGURE 18

MARCH SPILL TRAJECTORIES FOR SPILL LOCATION 1

TIDAL CURRENT ONLY

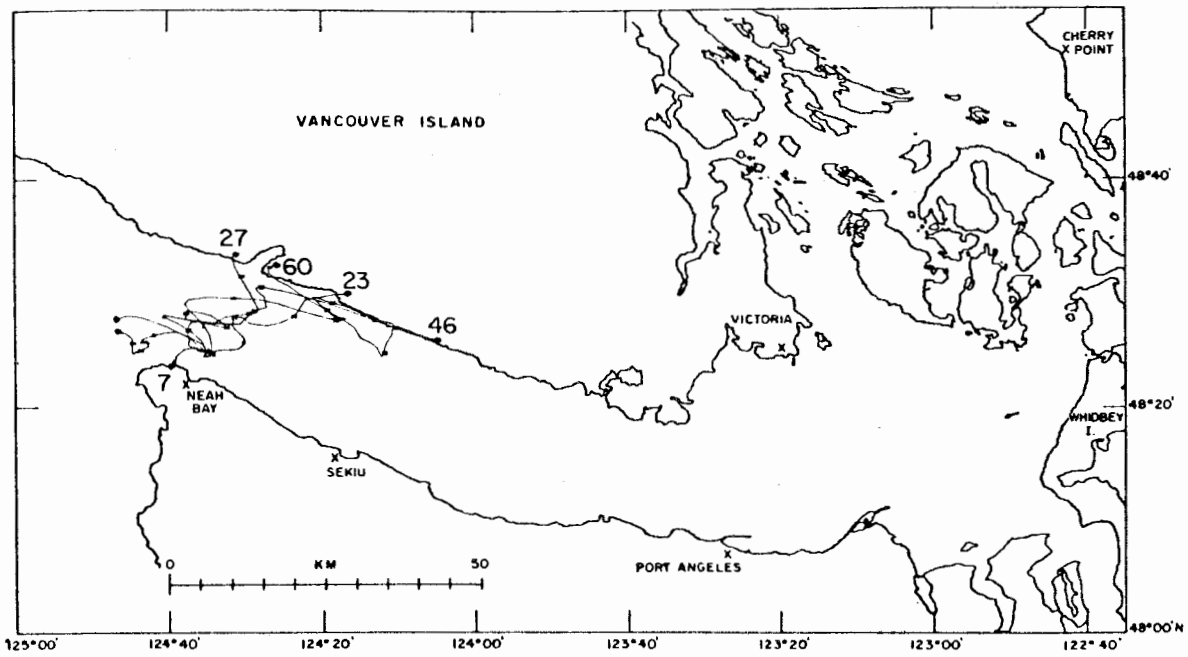

TIDAL CURRENT PLUS 10 CM/SEC

ESTUARINE CURRENT IN STRAITS

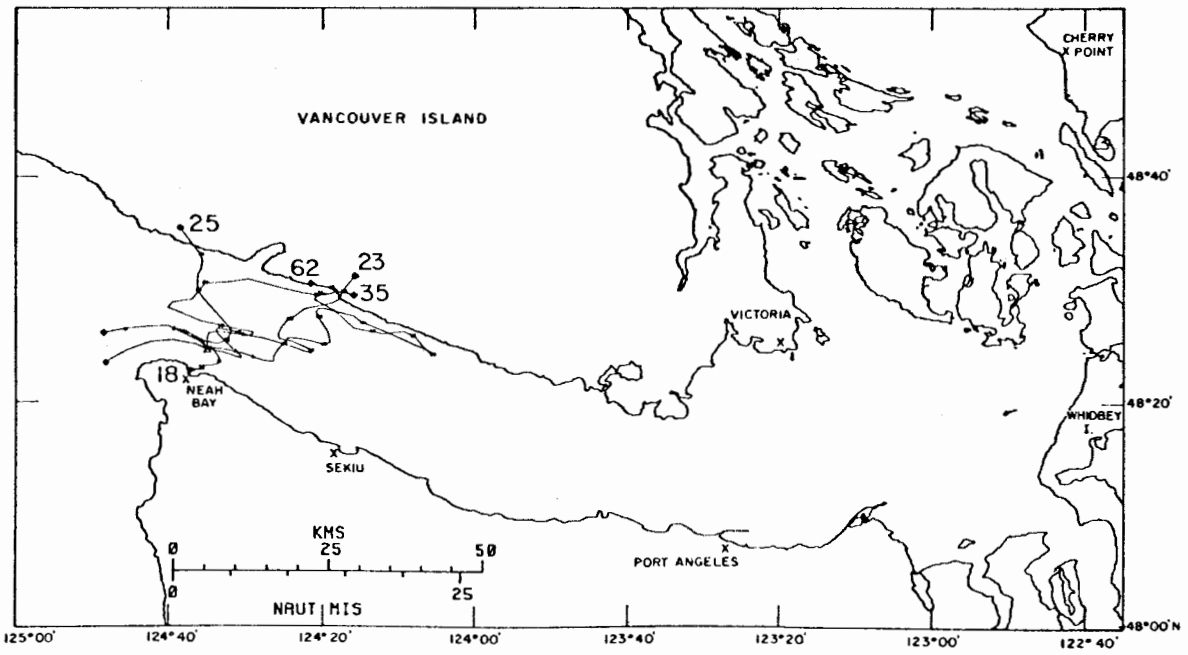

Times to Landfall (in Hours) Are Indicated Next to Impact Locations

FIGURE 19

SEPTEMBER SPILL TRAJECTORIES FOR SPILL LOCATION 1

TIDAL CURRENT ONLY

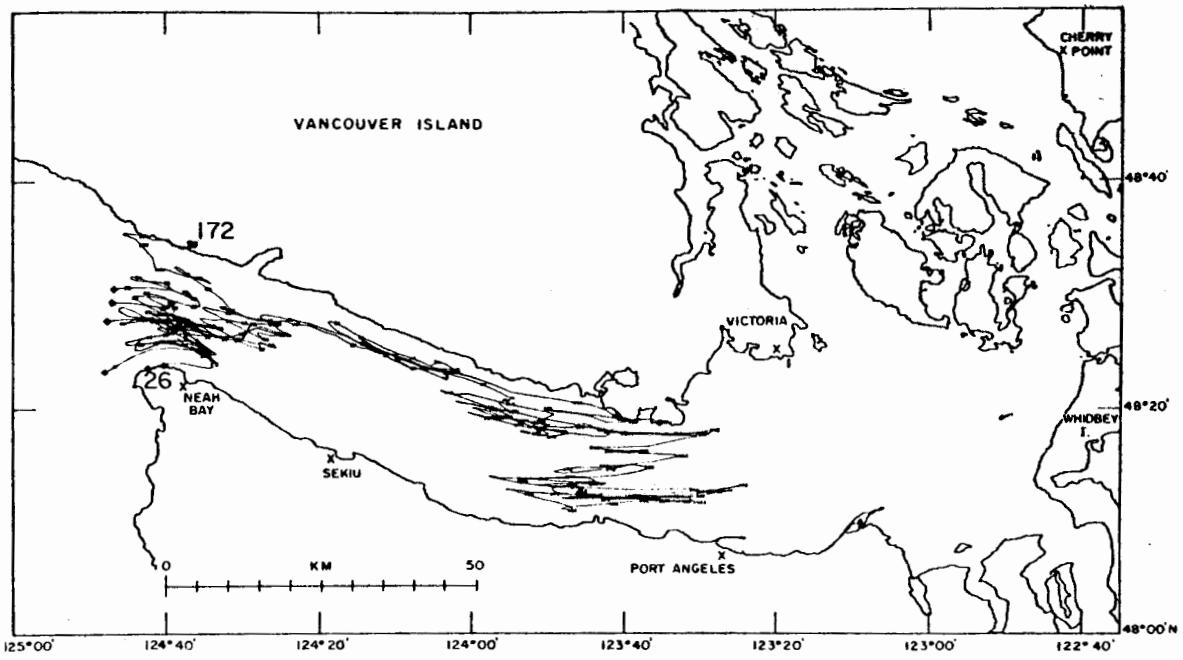

TIDAL CURRENT PLUS 30 CM/SEC

ESTUARINE CURRENT IN STRAITS

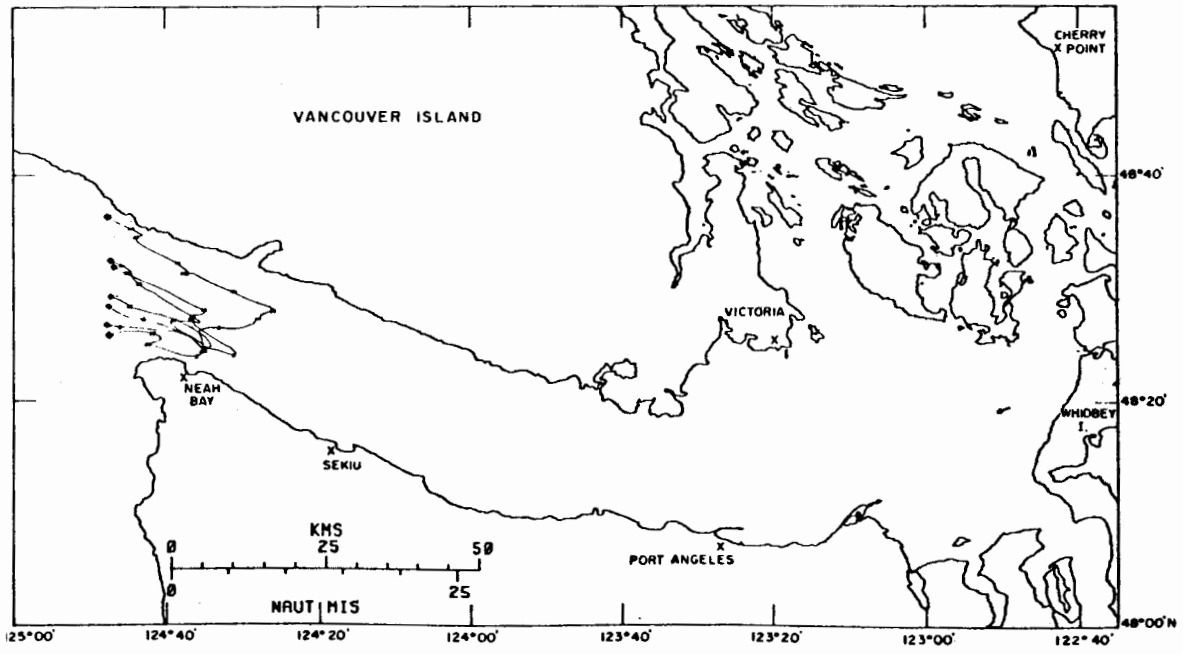

the interior Straits hitting both southern Vancouver Island from Race Rocks to the mouth of the Straits, and the Washington coast. Our results also show northerly and southerly impact zones. The effect of a 10 cm/sec estuarine flow for March is shown in the lower half of Figure 18. Notice that even with this steady seaward flow, one spill still progresses 30 kilometers into the Straits before the strong westerly wind dies, allowing the spill to be carried westward 15 kilometers towards the Straits entrance before it finally beaches. Typical trajectory times were 24 to 48 hours, although spills reached the U.S. shore in 16 hours, and the Canadian shore in as little as 23 hours.

There are no comparable drifter studies for this region for September. The stronger summer estuarine flow which persists into September was found to be of great importance to the trajectories. The upper half of 19 shows that under conditions of no estuarine flow, spills could be carried by the wind into the central basin. However, adding a steady current of 30 cm/sec (lower half 19) causes all the spills to be swept out the entrance. The proximity of the northern and southern most trajectories to Vancouver Island and Cape Flattery, respectively, indicates some probability of impact in these areas with the 30 cm/sec hypothesized estuarine flow. The effects of coastal pumping and an inflow in the southern portion of the Straits would appear to be to cause the coastal region west of Sekiu to be threatened. Of the two figures, the lower one is probably most analogous to real spill behavior. Characteristic times to shore are on the order of 10 hours to the U.S. coast and 30 hours to southern Vancouver Island.

5. SUMMARY AND CONCLUSIONS

Figure 20 summarizes our qualitative interpretation of the model results for several trajectory scenarios. The primary impact zones are shown in the shaded cones emanating from the hypothesized spill sites. These estimates are based on the considerations discussed above. The results of our experiments with the simulated spill trajectories under the purely tidal versus tide-plus-estuarine current assumptions demonstrated the highly dictomous behavior of the system. The estuarine current was clearly shown to be a key parameter in a trajectory, and it will require further consideration in any subsequent model development. For the time being, the coarse simulation used here will have to suffice.

We have also seen that the sea breeze can play a critical role in trajectories in the eastern part of the central basin. On days of strong seabreeze activity, spills can be carried south into Admiralty Inlet and perhaps onto Whidbey Island. The same spills on another day without the seabreeze would tend to move slowly north.

Finally, it should be recognized that this report does not encompass the effects of all of the known oil spill transport mechanisims. Foremost, we have completely neglected spreading. This was not out of oversight, but rather out of resignation. It is our opinion that the agreement between the few spreading theories and the scarce spreading data is so poor that little is to be learned by rewarming these old formulas. This is particularly true

FIGURE 20

QUALITATIVE INTERPRETATION OF RESULTS

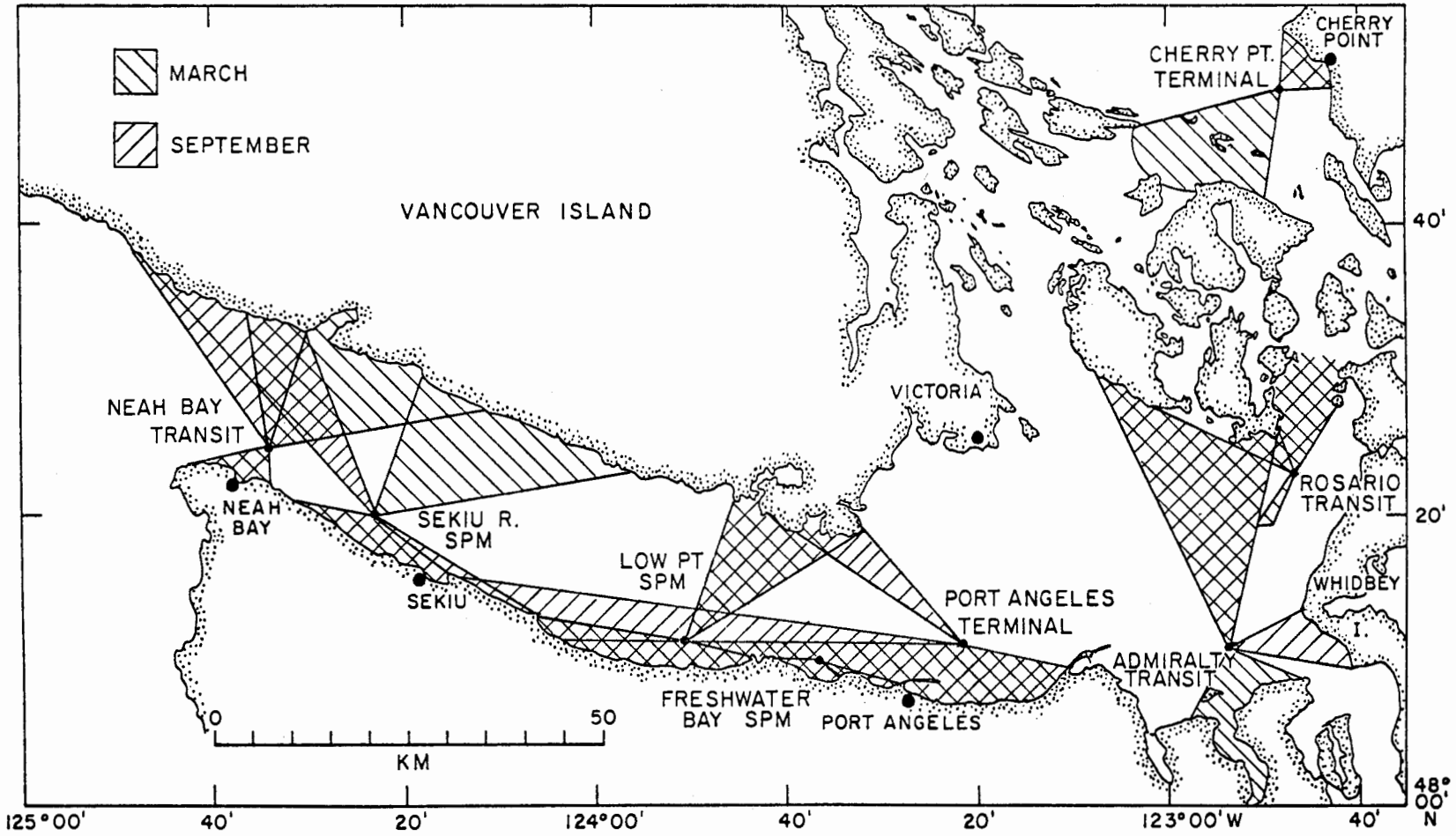

when these formulas are deeply imbedded in an already complex model.

Nor is this the only transport mechanism neglected. Following the first beaching of the spill, portions of the oil will be refloated and may be transported to other regions. This relaunching of the spill will generally occur on the rising, or flood stage of the tide. Thus, the tidal current is rectified insofar as the transport of the beached oil is concerned, and we can expect some net motion of the oil to the east along the beaches of the Strait.

Further work is needed to expand the number of wind cases to better represent the observed behavior in the region. The tide model should be expanded to include Puget Sound proper and additional case studies and verification should be made with the full trajectory model.

BIBLIOGRAPHY

Cannon, Glenn A. (ed.) 1978 "Circulation in the Strait of Juan de Fuca: Some Recent Oceanographic Observations." NOAA Technical Report ERL 399-PMEL 29, U.S. Dept. of Commerce, Environmental Research Laboratories, Boulder, Colorado (80303).

Holbrook, James R. (personal communication) Pacific Marine Environmental Laboratory, ERL, NOAA, Seattle, Washington (98105).

Maunder, W.J. 1968: "Synoptic weather patterns in the Pacific Northwest." Northwest Sci. 42, 2 80-88.

McGary, Noel and John H. Lincoln 1977 "Tide Prints, Surface Tidal Currents In Puget Sound" (Washington Sea Grant publication, WSG 7701) University of Washington, Department of Oceanography. Cont. No. 940 Seattle, Washington.

Overland, James E., Matthew H. Hitchman and Young-June Han, 1978 "A Regional Surface Wind Model for Mountainous Coastal Areas" ERL Technical Report 000-PMEL-000, U.S. Dept. of Commerce, Environmental Research Laboratories, Boulder, Colorado (80303).

Pease, Carol H. (in draft) An Empirical Tidal Model for the Puget Sound Region, ERL Technical Report.

Phillips, Earl L. 1968: Washington Climate for these counties, King, Kitsap, Mason, Pierce. Cooperative Extension Service, Washington State University, Pullman, Washington, 66 p.

Reed, Thomas R. 1931: "Gap winds of the Strait of Juan de Fuca." Mon. Wea. Rev. 59, 10, 573-576.

Schumacher, James D. and R.M. Reynolds 1974 "STD. Current Meter, and Drogue Observations in Rosario Strait, January-March 1974." NOAA Technical Report ERL 333-PMEL 24 U.S. Department of Commerce, Environmental Research Laboratories, Boulder, Colorado (80303).

Staley, D.O. 1957 "The Low-level Sea Breeze of Northwest Washington" J. of Met. (Now J. of Atmos. Science) Vol. 14, No. 5, pp 458-470.

ACKNOWLEDGEMENTS

We thank Mr. James R. Holbrook, of PMEL, who was most helpful in discussing his ongoing work and Dr. Richard Thomson, of the Institute of Ocean Science Environment Canada, at Patricia Bay, Canada, who provided us with the hourly wind data from Race Rocks.

The computations were completed with help from Betty-Ann Morse, Eric Raisters, Tom Hiester, and Mark Bjornson. Their diligence and patience greatly simplified the job of producing this report.

FIGURE CAPTIONS

Figure 1: Surface wind roses for Washington stations for January and July (adapted from Phillips, 1968).

Figure 2: Weather pattern L1 (adapted from Maunder, 1968).

Figure 3: Weather pattern L2 (adapted from Maunder, 1968).

Figure 4: Weather pattern H1 (adapted from Maunder, 1968).

Figure 5: Weather pattern H2 (adapted from Maunder, 1968).

Figure 6: Example of southwesterly geostrophic flow before the passage of a cold front on 08 December 1976.

Figure 7: Local wind field for 0000 GMT on 08 December 1976. One barb represents 10 kts and a half barb represents 5 kts.

Figure 8: Example of high pressure over the interior with low winds on 01 December 1976.

Figure 9: Local wind field for 0000 GMT on 01 December 1976.

Figure 10: Example of high pressure off the Oregon coast with northwesterly winds on 09 December 1976.

Figure 11: Local wind field for 1200 GMT on 09 December 1976.

Figure 12: Hodographs for July and August 1950 at Everett, Olympia, Seattle-Tacoma airport, Victoria and Port Angeles. The observations are valid 20 minutes past PST hours indicated. Solid lines and open circles represent July values and dashed lines and dots represent August (adapted from Staley, 1957).

Figure 13: Straits of Juan de Fuca and San Juan Islands tidal grid system (1 km resolution).

Figure 14: Regional surface winds induced by inland high pressure system.

Figure 15: Regional surface winds during storm passage.

Figure 16: Regional surface winds induced by east Pacific high pressure ridge.

Figure 17: Sea breeze wind field.

Figure 18: March spill trajectories for spill location 1.

Figure 19: September spill trajectories for spill location 1.

Figure 20: Qualitative interpretation of results.